Microstructure of accumulative roll bonded high purity aluminium laminates

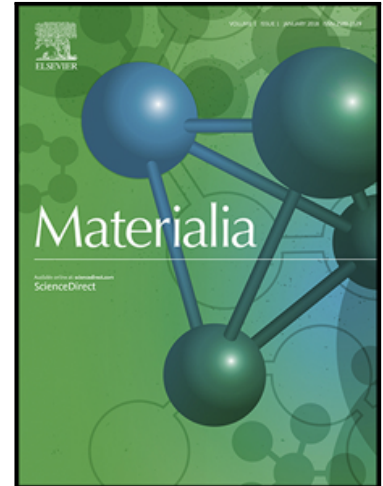Chekhonin, P.; Zöllner, D.; Zimmer, E.; Scharnweber, J.; Romberg, J.; Skrotzki, W.;

Accepted Manuscript

Microstructure of accumulative roll bonded high purity aluminium laminates

Paul Chekhonin , Dana Zöllner , Enrico Zimmer ,
Juliane Scharnweber , Jan Romberg , Werner Skrotzki

Please cite this article as: Paul Chekhonin , Dana Zöllner , Enrico Zimmer , Juliane Scharnweber , Jan Romberg , Werner Skrotzki , Microstructure of accumulative roll bonded high purity aluminium laminates, *Materialia* (2019), doi: https://doi.org/10.1016/j.mtla.2019.100236

Microstructure of accumulative roll bonded high purity aluminium laminates

Paul Chekhonin[1,2*], Dana Zöllner[1,3], Enrico Zimmer[1], Juliane Scharnweber[1], Jan Romberg[4], Werner Skrotzki[1]

[1] Institut für Festkörper- und Materialphysik, Technische Universität Dresden,
    D-01062 Dresden, Germany
[2] Helmholtz-Zentrum Dresden-Rossendorf, 01328 Dresden, Germany
[3] B CUBE – Center for Molecular Bioengineering, Technische Universität Dresden, 01307 Dresden, Germany
[4] Leibniz-Institut für Festkörper- und Werkstoffforschung,
    D-01069 Dresden, Germany

[*] corresponding author: p.chekhonin@hzdr.de

Keywords: accumulative roll bonding, microstructure, dynamic recrystallization, modelling

Abstract

Aluminium sheets of high purity were produced by accumulative roll bonding (ARB) at room temperature. The microstructure of the sheets up to 16 ARB cycles was analyzed by scanning electron microscopy. In all sheets discontinuous dynamic recrystallization occurred leading to coarse grains. In general, the grain size decreases with increasing number of applied ARB cycles, but remains much larger than the theoretical layer thickness after 6 or more ARB cycles. It is shown for the first time, how the interfaces introduced by ARB have a significant effect on the elongated grain shape by a combined experimental-numerical study: The resulting microstructure is qualitatively discussed with regard to defects introduced at the interfaces by the ARB process, while two-dimensional Potts model simulations yield very good qualitative agreements with the experiments and underpin the importance of the ARB interfaces as barriers for the motion of grain boundaries.

1. Introduction

Among different severe plastic deformation (SPD) methods, accumulative roll bonding (ARB) facilitates the production of high strength sheets and laminates [1,2,3]. Generally, the high strength results from a very high density of dislocations and grain boundaries that form during SPD. Typically, a steady state so-called ultra-fine grained (UFG) microstructure is

achieved after a high enough amount of deformation. When ARB is done on aluminium alloys or technical pure aluminium, in the steady state the grain size in sheet normal direction (ND) typically is in the range of some 100 nm and about 1 μm [4, 5, 6, 7, 8]. Furthermore, in comparison to the rolling direction (RD) and transverse direction (TD) the grain size or grain boundary spacing along ND is smaller by about a factor of two. The grain size is not significantly higher for aluminium with enhanced purity (99.99 wt.%) [9], as the main mechanisms responsible for the resulting microstructure in both cases are based on continuous dynamic recrystallization (CDRX). More details on CDRX are discussed elsewhere [10, 11, 12, 13].

In contrast to other SPD processes, additional defects may be introduced into the material by ARB. In many ARB studies oval shaped structures ("pockets") containing grains that are even finer in comparison to the surrounding area were observed at the bonding interfaces [14, 15, 16, 17]. Furthermore, under ambient conditions aluminium forms a few nm thick oxide layer [18]. Consequently, with any ARB pass another alumina layer is introduced into the sheet through the bonding interface. During a recent analysis of recrystallization and grain growth in ARB sheets of combined technical and high purity aluminium [17] it was observed that not only the pockets, but also pure bonding interfaces (without pockets) tend to hamper the grain boundary movement. To the best knowledge of the authors, so far no study exists dedicated to the influence of alumina at the bonding interfaces of aluminium sheets produced by ARB. Therefore, it is the main goal of this work to clarify the nature and the distribution of the alumina layer by using high purity aluminium (5N or 99.999 wt.% Al) for ARB. With the low impurity content the grain boundary mobility is generally very high [19] and discontinuous dynamic recrystallization (DDRX) may already appear at comparably low temperatures or even at ambient temperature. Previous publications demonstrated the occurrence of DDRX in 5N aluminium at ambient temperature [20, 21, 22]. In ARB sheets made of 5N Al the migration of grain boundaries is expected to be only influenced by the above mentioned

2

pockets and alumina layers. Therefore, a microstructural analysis of such sheets may allow drawing conclusions with respect to the distribution of these defects.

2. Experimental procedure

Cold rolled 5N high purity aluminium sheets with a thickness of 0.8 mm were annealed at 500°C for one hour. From ref. [22] it is known that annealing of 5N sheets of comparable dimensions under similar annealing conditions leads to a grain size of several mm.

After wire brushing the sheets were roll bonded at ambient temperature by a four-high rolling mill (IFW Dresden) with a per pass reduction of 50% and a rolling speed of 20 m/min. The rolls had a diameter of 110 mm. Sheets with one to 16 ARB cycles were produced without lubrication. The sheet thickness became smaller with increasing number of ARB cycles, after 14 or more ARB cycles it decreased to about 0.7 mm. This may be explained by the width of the processed sheets which also decreased from about 8 cm after 2 ARB cycles to about 4 cm after 16 ARB cycles due to trimming. Consequently, the pressure from the rolling mill increased, assuming that the force provided by the rolling mill remained the same.

Microstructural investigations were carried out by a Zeiss ULTRA 55 scanning electron microscope (SEM) with an acceleration voltage of 20 kV applying secondary electron (SE) and backscatter electron (BSE) imaging on the ND-RD planes.

The average grain boundary spacing was determined by the line intercept method applied to the BSE images. The imaging was done on large areas of at least 4 mm² containing at least 500 grain boundaries along the intercept lines for RD as well as for ND. Few non-recrystallized areas were disregarded in this analysis. For SEM investigations the surface was prepared by mechanical grinding (2400 grid wet SiC-paper as last step) and electro-polishing at 42 V. The electrolyte consisted of 9 vol.% perchloric acid in 91 vol.% ethanol and was cooled to about −15°C.

3

3. Numerical procedure

About 35 years ago, the first computer simulation algorithms were developed to model recrystallization and grain growth in polycrystalline materials at thermal treatment. Tailoring different applications, various types of simulations were developed on different size and time scales from atomistic simulations to mesoscopic ones, where the latter works on the microstructural level. The latter type permits a very selective tailoring of material parameters, enables an analysis of large grain structures over long time spans, and finally facilitates comparisons with experiments. As a consequence, for mesoscopic size scales different models were produced over the years, such as the Monte Carlo Potts model, Surface Evolver, phase-field method and vertex method (cf. [23] and the references within).

Among the mentioned methods the Monte Carlo Potts model is distinct for its comparative simplicity. Nevertheless, it can be modified to tailor and model complex problems such as the influence of texture and second phase particles on grain growth, or recrystallization in specific materials such as aluminium alloys and steels [24].

In the Potts model sharp interfaces and therewith grain boundaries are assumed. Typically, two material parameters characterize the grain boundary, its mobility m and energy per unit length γ. Generally, both parameters depend on the misorientation between two adjacent grains. However, this dependence is neglected in the present work as the focus is purely on the basic recrystallization process. Furthermore, the Potts model requires a given initial microstructure. In the present work, the initial microstructure defined by grain size distribution of a specific number of grains, including their topology and grain orientation is projected onto a quadratic two-dimensional lattice with N lattice points. For a given point in

4

the quadratic lattice eight nearest neighbours (*nn* = 8) are considered for local interactions. For the edges of the lattice specific application dependent boundary conditions have to be considered. In the present case, periodic boundary conditions in rolling direction and free boundary conditions in normal direction were implemented. The latter treats the top-most and bottom layers as surfaces.

In the present computing algorithm the smallest time unit (one Monte Carlo Step (MCS)) consists of *N* reorientation attempts. Each reorientation attempts includes the following routine:

1. In a randomly picked lattice point a new state is generated by changing its orientation to the orientation of one of its neighbouring points (thus nucleation of new orientations is prohibited).

2. The energy of both, the old and the new state is calculated by the Hamiltonian

$$H = \frac{1}{2} \sum_{i=1}^{N} \sum_{j=1}^{nn} \gamma \left(1 - \delta(Q_i, Q_j) \right) + \mathcal{H}_i \tag{1}$$

Where the interaction of the *i*-th lattice point with all its neighbours is measured by the specific grain boundary energy per unit length γ. For equal neighbouring orientations Q_i and Q_j the Kronecker delta function is equal to one, and zero for different neighbouring orientations. Therefore, only different orientations provide a contribution. The variable $\mathcal{H}_i$ characterizes the stored energy of the lattice point − showing a clear difference between recrystallized and not recrystallized lattice points.

3. The final orientation of the chosen lattice point is determined by a probability of

$$p = \frac{m}{m_{\max}} \frac{\gamma}{\gamma_{\max}} \cdot exp \left(\frac{-\Delta E}{k_B T} \right) \quad \text{if} \quad \Delta E > 0 \tag{2}$$

and

$$p = \frac{m}{m_{\max}} \frac{\gamma}{\gamma_{\max}} \quad \text{if} \quad \Delta E \leq 0 \tag{3}$$

where *m* is the previously stated grain boundary mobility. The simulation thermal energy (so-called simulation temperature) is expressed through $k_B T$, which has to be selected with care

5

such that unphysical lattice effects are prevented [25]. The maximum values of specific grain boundary energy and mobility are given by the constants γ_{max} and m_{max} , respectively. Assuming normal grain growth (where merely high angle grain boundaries with identical properties contribute to coarsening), leads to $m = m_{max}$ and $\gamma = \gamma_{max}$. More details are provided in the review articles [23, 25] and the references within.

The aim of the simulation is to focus on the basic principles of recrystallization in the microstructure as shown in Fig. 1 in the ND-RD plane of the rolled sheets. For experimental input into the simulation, there are no images available showing the initial microstructures before recrystallization. However, in Fig. 1 (white arrows) non-recrystallized areas may be observed showing a very fine grained structure. Hence, as a starting point for all simulations initially fine grains have been assumed and 2-dimenstional layered grain microstructures were digitally generated depending on the number of layers for the different ARB cycles (Fig. 6a). All grains have a distinct orientation. However, here for all boundaries it is assumed that the grain boundary energies and mobilities have identical low values leading to a persistence of the fine grains in non-recrystallized regions Additionally, thin interlayers are introduced, which have a height of one lattice point and span the whole width of the sample (thin red lines in Fig. 6a). These interlayers represent the alumina layers introduced by ARB. However, to be more precise, it is necessary to classify different ARB bonding interfaces. To do so, a unitless parameter "age" is introduced. The most recent bonding interface at the centre thickness of the sheet has the age of 1, the interfaces originating from the previous ARB cycle located at the quarter thickness of the sheet have an age of 2, etc. The term "age" must not be confused with the aging phenomenon in Al-allows, which is a completely unrelated issue.

In the applied model it is assumed that the interlayers are broken up as follows:

- The interlayer of age 1 is broken up approximately equidistantly, where the length of the broken and unbroken parts vary slightly.

- In the interlayer of age 2, the formerly broken-up parts double in length as do the unbroken parts, since the layer increases its length during rolling by a factor of two. However, the formerly unbroken sections now also break up in two smaller parts.

- This procedure is repeated for all interlayers of higher age.

For the recrystallization, new seeds (representing nuclei) are randomly generated at grain boundaries or interlayers. Each seed has an initial size of 2×2 lattice points – which is negligible in comparison to the layer thickness between 13 lattice points (after 6 ARB cycles) and 400 lattice points (after 1 ARB cycle). The number of seeds starts with one seed per time step (or per Monte Carlo unit (MCU)) for a simulation of sheets after 2 ARB cycles, but increases slightly with increasing number of ARB cycles proportional to the additional interfaces. The stored energy $\mathcal{H}$ inside these seeds is significantly lower in comparison to the initial microstructure by a factor of 10, which has been derived numerically by a parameter variation. Furthermore, the newly formed grain boundaries have significantly higher values for grain boundary energy and mobility than the existing ones, which have also determined by parameter variations. For graphical representations in Figs. 6 and 7, the pre-existing boundaries with low energy and mobility are represented in red, whereas the newly formed recrystallized grains with high energy and mobility are enclosed by blue boundaries. Here it should be mentioned that in agreement to a previous study [22] only the nucleation process is taking place during DDRX, while the major recrystallization is classified as static recrystallization. Hence, in the implemented model DDRX is neglected and only static recrystallization is considered.

4. Results and discussion

Figure 1 shows BSE images of the 5N ARB sheets after different deformation stages. Experimental results presented in a previous publication [22] indicate that applying ARB to 5N Al results in DDRX during deformation followed by some subsequent static recrystallization leading to a coarse grained microstructure. In general, the same mechanism

7

may explain the observed recrystallized microstructure here. Only a few non-recrystallized areas marked by white arrows in Fig. 1 remained. Pockets can be observed in the ARB interfaces and their number obviously increases in sheets with higher ARB cycle numbers. Measurements performed by energy dispersive X-ray spectroscopy (not presented here) indicate traces of oxygen in these pockets. This may be attributed to small aluminium-oxide (alumina) particles in their inside (Fig. 2). Their presence leads to particle strengthening and hampering of grain boundary migration. This may explain why these areas do not exhibit DDRX and appear to be persistent with further deformation.

Figure 3 presents the average grain boundary spacing and non-recrystallized area fraction as a function of the number of ARB cycles. For ND and RD until 8 ARB cycles the grain boundary spacing decreases stronger than afterwards. While after 2 ARB cycles the coarse grains are mostly limited to one specific layer (here a layer is defined as the volume between two adjacent bonding interfaces), the BSE contrast indicates that many grains overstep these interfaces after 4 or more ARB cycles (Fig. 1). Similar to what was reported in [17], Fig. 1 qualitatively demonstrates that in the sheets after any number of ARB cycles the bonding interface with an age of 1 almost always acts as barrier for grain boundaries. The higher the age of the bonding interface, the more likely this interface is crossed by grain boundaries. This is demonstrated in Fig. 4 showing the interface fraction crossed by grain boundaries (or more precisely, the fraction where in the BSE micrograph the gray value below and above the interface is the same) as a function of age in a sheet processed with 4 ARB cycles (determined by line intercept method). While the fraction of ARB interfaces overstepped is about 6% at an age of 1, this value increases monotonously to 40% at an age of 4. To extract corresponding data on sheets with higher cycle numbers and accordingly for interfaces of higher age is difficult, because it is not possible to accurately spot the traces of ARB interfaces anymore. However, the percentage will definitely increase further, because the grain boundary spacing does not decrease much after 8 or more ARB cycles.

The alumina particles are not only present in the pockets but presumably with a much lower density at any ARB interface. To support this claim, Fig. 5a shows an interface with an age of 4. While at the right side of Fig. 5a the interface simultaneously is a grain boundary, at the left side of the image the interface (marked by a red dashed line) obviously is overstepped. Figures 5b and c show parts of the interface not overstepped using a very surface sensitive SEM Inlens SE detector at high magnification. The interface was etched to some extent by the electro-polishing procedure. A few particles (presumably alumina) can be recognized in Fig. 5c (marked by black arrows), while this is not the case in Fig. 5b. On the other hand, as is demonstrated on another specimen position in Fig. 5d, an interface may appear to be overstepped even in the presence of pockets (marked by a blue arrow). This indicates that originally overstepping of ARB interfaces first takes place in areas with low particle density. Subsequently, the boundary expands into the neighbouring layer along ND until it meets another interface, and additionally, the boundary also expands along TD and RD until it meets another grain boundary.

Qualitatively, the data presented in Figs. 3a, 4 and 5 can be understood by means of alumina particle distribution in the high purity sheets. In the following it will be assumed that the driving force P_D for DDRX (and presumably subsequent static recrystallization) is only attributed to the deformed matrix and that any grain boundary movement stops when it meets another grain boundary. Thus, grain growth after DDRX is excluded.

In general, alumina particles from the ARB process will lead to a Zener pinning force P_Z [19]

$$P_Z \sim \frac{F_V \gamma}{r} \tag{4}$$

where F_V is the volume fraction of randomly distributed spherical particles with radius r and γ is their specific interface energy. If P_Z exceeds P_D the boundary movement comes to a halt. With every additional ARB cycle the area of a certain ARB interface will increase by a factor of two, while the number and size of particles remains the same, so that F_V and consequently

P_Z is halved at this interface, while the deformation degree and with it P_D remains similar after each cycle. Hence, if the distribution of the particles would be homogeneous (equidistant) the fraction of the interfaces overstepped should change abruptly after a certain age, when P_D exceeds P_Z. However, the overstep fraction presented in Fig. 4 is increasing gradually. Therefore, an inhomogeneous particle distribution may explain the observations stated. With an inhomogeneous particle distribution there is a certain probability to overstep the interface after any age and qualitatively this probability increases with higher age.

In order to underpin these experimental findings and the corresponding explanations given, two-dimensional Potts model simulations have been performed according to the above description.

The microstructural evolution for a sheet after four ARB cycles is presented in Fig. 6 for five different annealing times. The representation analogously to Fig. 1 in the ND-RD plane shows the recrystallization behaviour spanning the different interlayers. In contrast to the experimental measurements, here we can get additional insights into the temporal development of the microstructures showing growth of recrystallized grains as well as impingement of such grains on the interlayers as well as on one another. The impingement characterizes a state, where the driving force for boundary motion has practically reduced to zero.

For a better comparison with experiment, the simulation has been performed four times for different numbers of ARB cycles, namely for 2, 3, 4, and 5 cycles, of which the result is shown in Fig. 7 for the fully recrystallized state. It can be seen that there are drastic changes in the microstructures with increasing number of ARB cycles in agreement with Fig. 1, although in the simulation we have more idealized conditions, e.g., perfectly horizontal and equidistant interlayers. Nevertheless, an analysis of the grain boundary spacing as a function of the number of ARB cycles for RD as well as for ND, as given in Fig. 8, shows a striking

qualitative similarity to the experimental measurement in Fig. 3a. In both cases the decrease in boundary spacing with increasing number of cycles can be observed, where the spacing in ND is visibly smaller than in RD. Also in both figures, the theoretical layer thickness crosses the two graphs within the observed regime (between 2 and 5 ARB cycles).

The above mentioned advantage of the simulation is among others due to the fact that we can plot temporal evolutions of most parameters. This has been done in Fig. 9 for the non-recrystallized area fraction as a function of the number of ARB cycles. In general, the non-recrystallized area fraction increases with increasing number of ARB cycles if the data are compared after the same annealing time spans. In addition, the relation is shifted to smaller values of area fractions with increasing time. Both observations make perfect sense. A higher number of ARB cycles means that more interlayers prevent the free motion of the recrystallized grains. Hence, their boundaries will more likely move in RD and TD making it more complicated to reach certain non-recrystallized areas. Of course, over time the remaining non-recrystallized parts are reduced in size yielding for long annealing times fully recrystallized samples as in Fig. 7. The disagreement with the experimental observation (where few non-recrystallized parts remain even after years) can be understood as follows: Local variations of driving pressure and annealing temperature (due to some adiabatic heating during deformation) presumably are responsible for the presence of non-recrystallized parts, e.g. at some point the grain boundaries stop completely. These effects were not considered in the present model.

Finally, Fig. 10 shows the fraction of ARB interfaces that have been crossed by a grain boundary as a function of their age. Here again a very good qualitative agreement when comparing simulation with experiment (Fig. 4) can be observed. There is a clear, seemingly linear, increase of the interface overstepped fraction on the age of the ARB interfaces.

All in all, the simulations performed underpin the experimental results and theoretical explanations given above. It can be concluded that the ARB interfaces act indeed as barriers

for grain boundary migration, while the stored energy in the non-recrystallized grain microstructure is the main driving force for the boundary motion. Once the microstructure is recrystallized coarsening practically stops.

Nevertheless, the authors would like to mention that even though there is a very good qualitative agreement between experiment and model, for a valuable quantitative comparison it would be necessary to extract material parameters like stored energy, grain boundary energies, and grain boundary mobilities, and then to incorporate them into the simulation. However, such an extraction is at least not easy to perform.

5. Conclusions

The present work is dedicated at some unexplored yet very important aspects pertaining to Accumulative Roll Bonding of aluminium. It examines the microstructural development of high purity aluminium sheets produced by ARB at room temperature. The major results can be summarized as follows:

1)

With the exception of a small area fraction discontinuous dynamic recrystallization occurred in all sheets leading to coarse grains.

2)

With increasing number of applied ARB cycles, the grain boundary spacing decreases, yet it remains much larger than the theoretical layer thickness after 6 or more ARB cycles. In comparison to the first 8 ARB cycles, the decrease slows down significantly after more than 8 ARB cycles.

3)

The ARB interfaces consist of irregularly distributed pockets and single alumina particles, which in general act as barriers for grain boundary migration. Their irregular distribution is

deduced from the interface fraction crossed by grain boundaries after different stages in the ARB processing.

4)

The experimental results compare very well with numerical simulations from a qualitative point of view. In particular, the simulations underpin the importance of the ARB interfaces as barriers for the motion of grain boundaries and show that the stored energy in the non-recrystallized grain microstructure is the main driving force.

Acknowledgments

References

[1]
Y. Saito, N. Tsuji, H. Utsunomiya, T. Sakai, R.G. Hong, Ultra-find grained bulk aluminium produced by accumulative roll-bonding (ARB) process, Scripta Mater. 39 (1998) 1221–1227.

[2]
Y. Saito, H. Utsunomiya, N. Tsuji, T. Sakai, Novel ultra-high straining process for bulk materials – development of the accumulative roll-bonding (ARB) process, Acta Mater. 47 (1999) 579–583.

[3]
N. Tsuji, Fabrication of Bulk Nanostructured Materials by Accumulative Roll Bonding (ARB), in: M.J. Zehetbauer, Y.T. Zhu (Eds.), Bulk Nanostructured Materials, 1st ed, Wiley-VCH, Weinheim, 2009, chap. 10.

[4]

N. Tsuji, T. Toyoda, Y. Minamino, Y. Koizumi, T. Yamane, M. Komatsu, M. Kiritani, Microstructural change of ultrafine-grained aluminium during high-speed plastic deformation, Mater. Sci. Eng. A 350 (2003) 108–116.

[5]
H.W. Höppel, J. May, M. Göken, Enhanced Strength and Ductility in Ultrafine-Grained Aluminium Produced by Accumulative Roll Bonding, Adv. Eng. Mater. 6 (2004) 781–784.

[6]
J. Scharnweber, W. Skrotzki, C.-G. Oertel, H.-G. Brokmeier, H.W. Höppel, I. Topic, J. Jaschinski, Texture, Microstructure and Mechanical Properties of Ultrafine Grained Aluminium Produced by Accumulative Roll Bonding, Adv. Eng. Mater. 12 (2010) 989–994.

[7]
M. Ruppert, W. Böhm, H. Hguyen, H.W. Höppel, M. Merklein, M. Göken, Influence of upscaling accumulative roll bonding on the homogeneity and mechanical properties of AA1050A, J. Mater. Sci. 48 (2013) 8377–8385.

[8]
M.S. Mohebbi, A. Akbarzadeh, B.H. Kim, S.-K. Kim, Analysis of Strain Rate Sensitivity of Ultrafine-Grained AA1050 by Stress Relaxation Test, Metall. Mater. Trans. A 45 (2014) 5442–5450.

[9]
N. Kamikawa, N. Tsuji, X. Huang, N. Hansen, Quantification of annealed microstructures in ARB processed aluminium, Acta Mater. 54 (2006) 3055–3066.

[10]
T. Hebesberger, H.P. Stüwe, A. Vorhauer, F. Wetscher, R. Pippan, Structure of Cu deformed by high pressure torsion, Acta Mater. 53 (2005) 393–402.

[11]
A. Vorhauer, R. Pippan, On the Onset of a Steady State in Body-Centered Cubic Iron during Severe Plastic Deformation at Low Homologous Temperatures, Metall. Mater. Trans. A 39 (2008) 417–429.

[12]
T. Sakai, A. Belyakov, R. Kaibyshev, H. Miura, J.J. Jonas, Dynamic and post-dynamic recrystallization under hot, cold and severe plastic deformation conditions, Prog. Mater. Sci. 60 (2014) 130–207.

[13]
J. Scharnweber, P. Chekhonin, C.-G. Oertel, J. Romberg, J. Freudenberger, J. Jaschinski, W. Skrotzki, Microstructure, Texture, and Mechanical Properties of Laminar Metal Composites Produces by Accumulative Roll Bonding, Adv. Eng. Mater. (2018) 1800210.

[14]
C. Kwan, Z. Wang, Microstructure evolution upon annealing of accumulative roll bonding (ARB) 1100 Al sheets materials: evolution of interface microstructures, J. Mater. Sci. 43 (2008) 5045–5051.

[15]
C.C.F. Kwan, Z. Wang, Cyclic deformation behavior of ultra-fine grained copper processed by accumulative roll-bonding, Procedia Engineering 2 (2010) 101–110.

[16]
O.V. Mishin, Y.B. Zhang, A. Godfrey, The influence of multiscale heterogeneity on recrystallization in nickel processed by accumulative roll bonding, J. Mater. Sci. 52 (2017) 2730–2745.

[17]
L. Lienshöft, P. Chekhonin, D. Zöllner, J. Scharnweber, T. Marr, T. Krauter, H.W. Hoeppel, W. Skrotzki, Static recrystallization and grain growth of accumulative roll bonded aluminium laminates, J. Mater. Res. 32 (2017) 4503–4513.

[18]
J. Evertsson, F. Bertram, F. Zhang, L. Rullik, L.R. Merte, M. Shipilin, M. Soldemo, S. Ahmadi, N. Vinogradov, F. Carlà, J. Weissenrieder, M. Göthelid, J. Pan, A. Mikkelsen, J.-O. Nilsson, E. Lundgren, The thickness of native oxides on aluminium alloys and single crystals, Appl. Surf. Sci. 349 (2015) 826–832.

[19]
F.J. Humphreys, M. Hatherly, Recrystallization and related annealing phenomena, 2nd ed. Elsevier, Oxford, 2004.

[20]
M.E. Kassner, H.J. McQueen, J. Pollard, E. Evangelista, E. Cerri, Restoration mechanisms in large-strain deformation of high purity aluminium at ambient temperature, Scripta Met. Mater. 31 (1994) 1331–1336.

[21]
W. Skrotzki, N. Scheerbaum, C.-G. Oertel, H.-G. Brokmeier, S. Suwas, L.S. Tóth, Recrystallization of high-purity aluminium during equal channel angular pressing, Acta Mater. 55 (2007) 2211–2218.

[22]
P. Chekhonin, B. Beausir, J. Scharnweber, C.-G. Oertel, T. Hausöl, H.W. Höppel, H.-G. Brokmeier, W. Skrotzki, Confined recrystallization of high-purity aluminium during accumulative roll bonding of aluminium laminates, Acta Mater. 60 (2012) 4661–4671.

[23]
D. Zöllner, A Potts model for junction limited grain growth, Comput. Mater. Sci. 50 (2011) 2712–2719.

[24]
K. Adam, D. Zöllner, D.P. Field, 3D microstructural evolution of primary recrystallization and grain growth in cold rolled single-phase aluminum alloys, Modelling Simul. Mater. Sci. Eng. 26 (2018) 035011.

[25]
D. Zöllner, A new point of view to determine the simulation temperature for the Potts model simulation of grain growth, Comput. Mater. Sci. 86 (2014) 99–107.
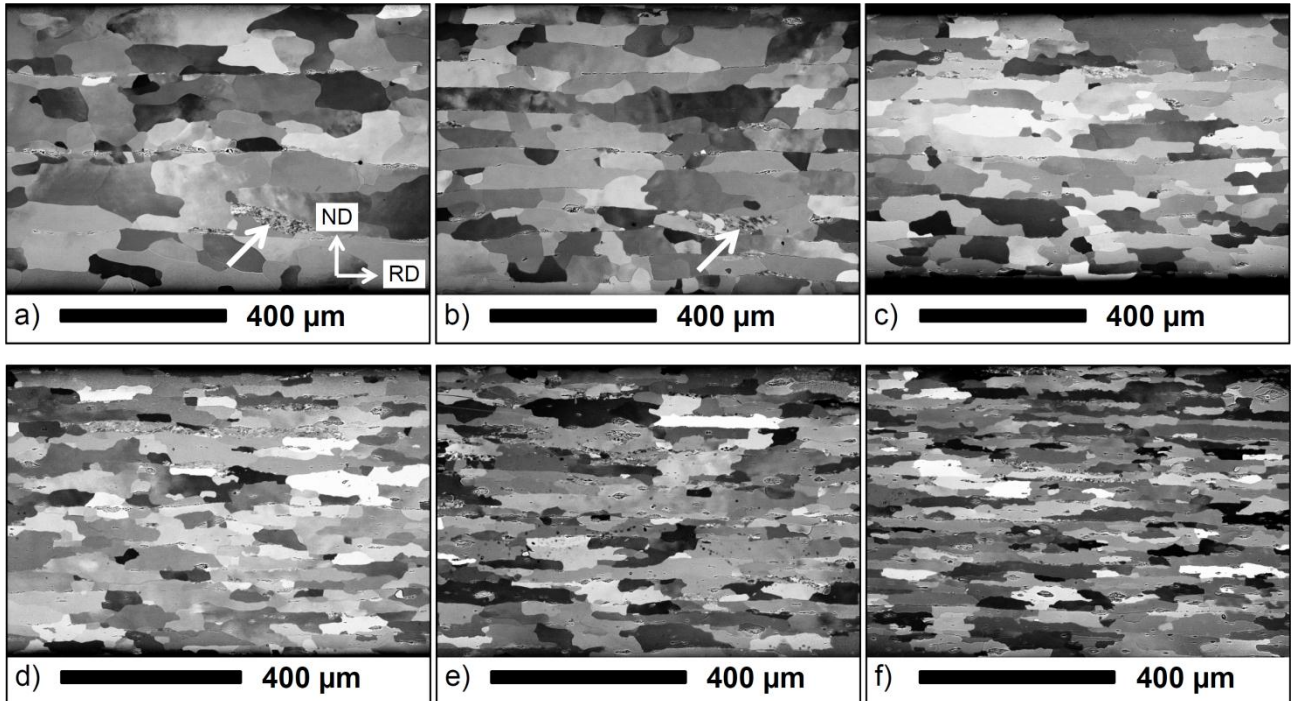
Graphical abstract
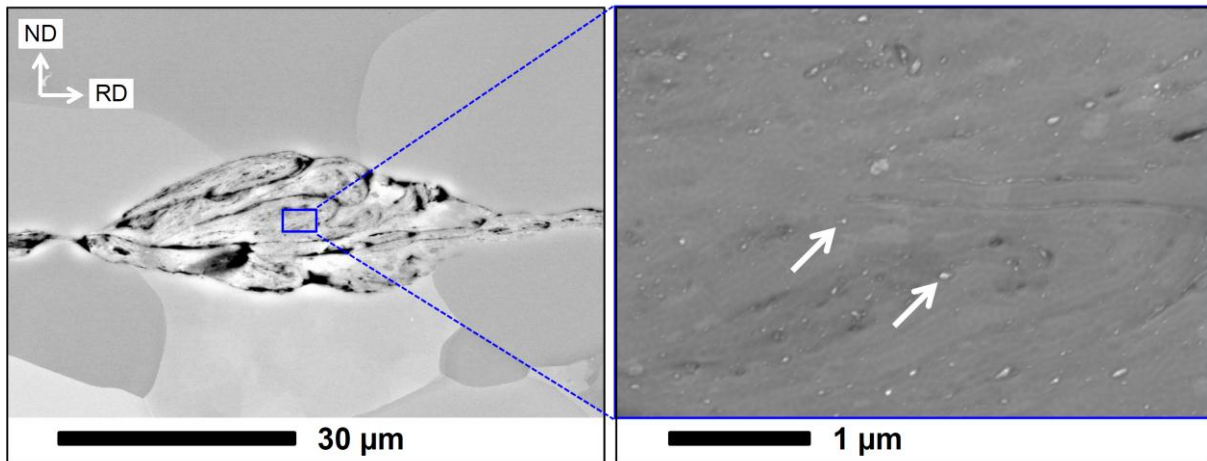
Declarations of interest: none

Figure 1: BSE images of the sheets after a) 2, b) 4, c) 6, d) 8, e) 12 and f) 16 ARB cycles.The high purity aluminium is recrystallized, only few non-recrystallized areas remain (white arrows).
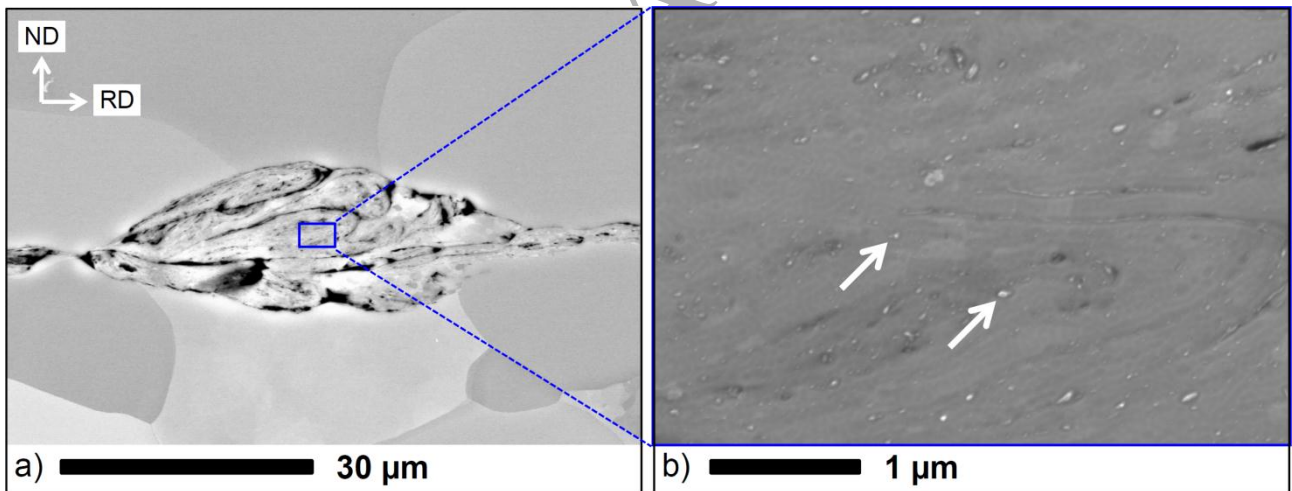

Figure 2: a) BSE image of a "pocket" in a sheet after 4 ARB cycles. b) shows an excerpt with higher magnification (SE contrast). The white arrows mark some of the alumina particles.
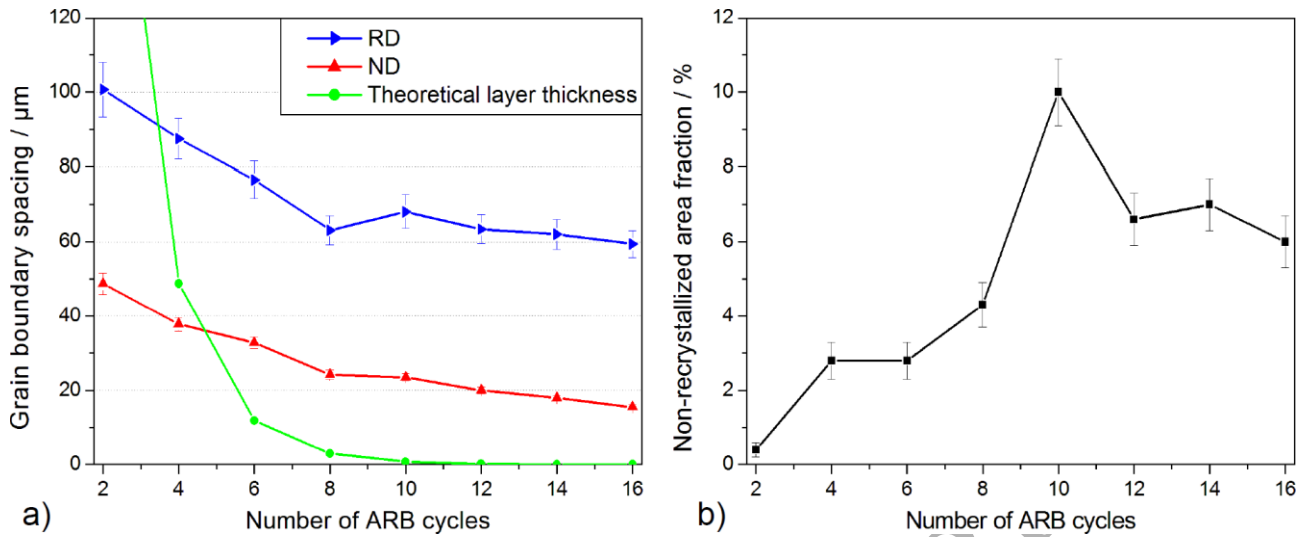
Figure 3: a) Average grain boundary spacing in RD and ND compared with the theoretical layer thickness and b) non-recrystallized volume fraction as a function of applied ARB cycles.
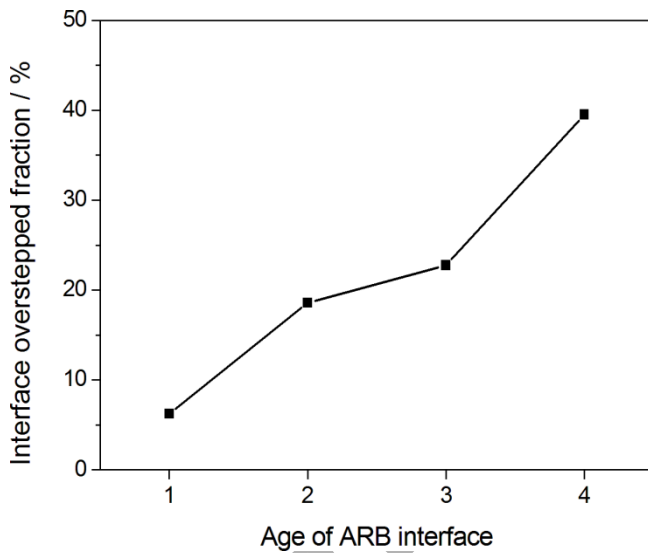
Figure 4: Fraction of ARB interfaces crossed by grain boundaries as a function of their age.
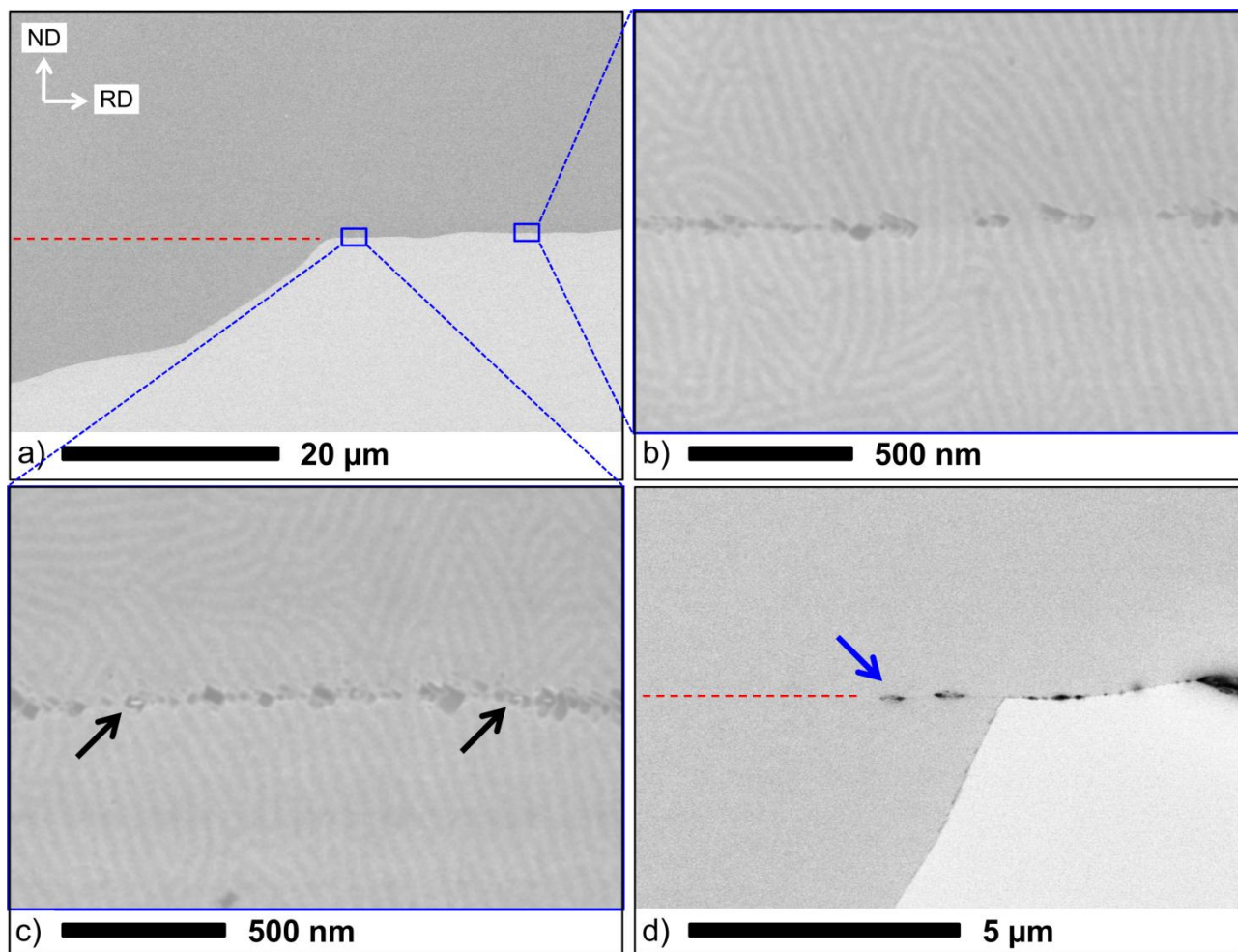
Figure 5: a) BSE image of an interface with an age of 4.The part of the interface which is overstepped is marked by a red dashed line. b) and c) excerpts of the same interface recorded with an Inlens SE detector at high magnification; particles in the interface are marked by black arrows. d) BSE image of another interface (also age of 4). The part of the interface which is overstepped is marked by a red dashed line, pockets are marked by a blue arrow.
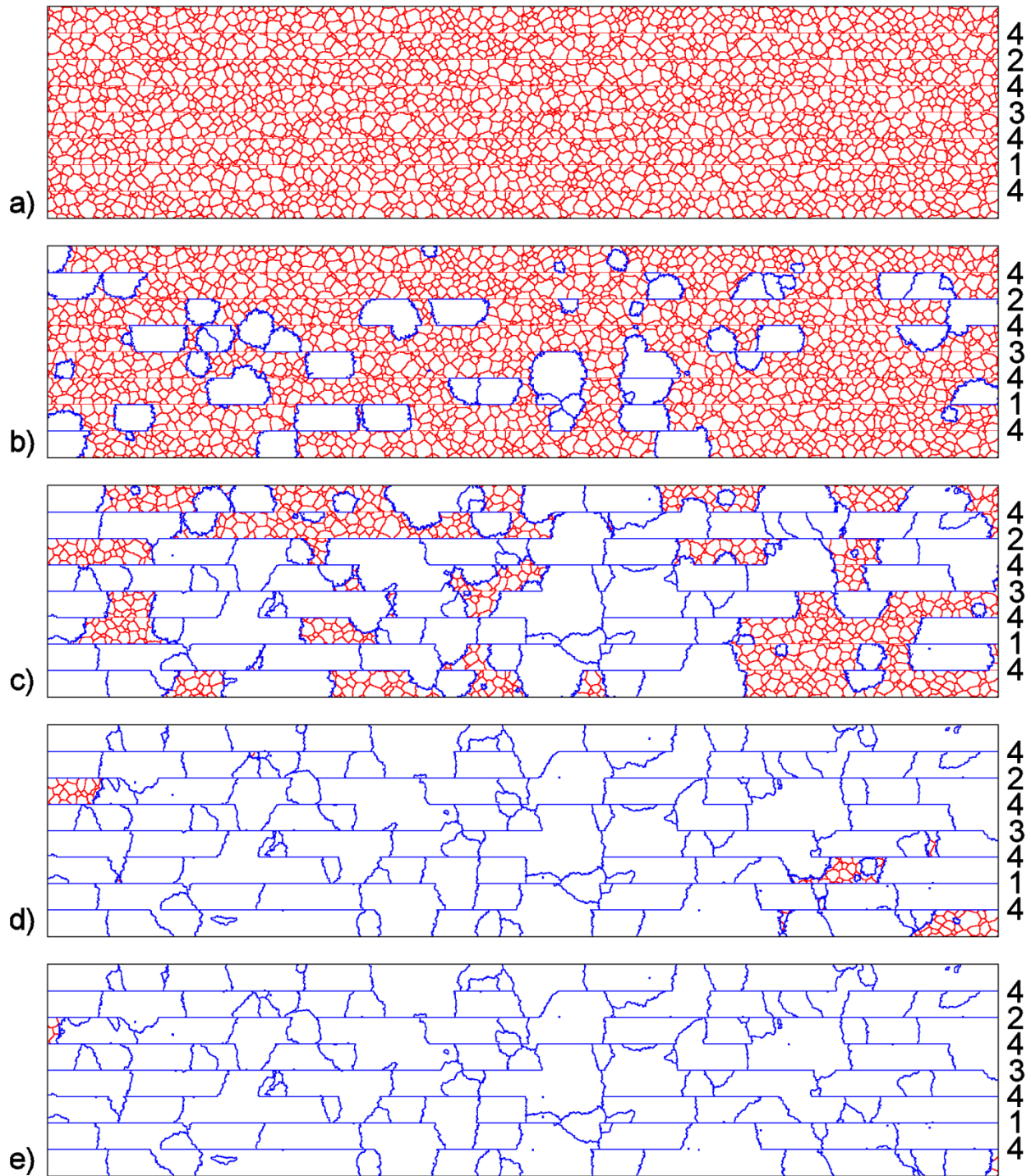
19

Figure 6. Temporal development of simulated sheets after 4 ARB cycles at a) $t = 0$ MCS, b) $t = 100$ MCS, c) $t = 200$ MCS, d) $t = 300$ MCS, and e) $t = 400$ MCS. Horizontal axis is RD, vertical is ND. The red boundaries mark grains of the non-recrystallized matrix, while recrystallized grains are enclosed by blue boundaries. The numbers on the right hand side denote the age of the ARB interfaces.
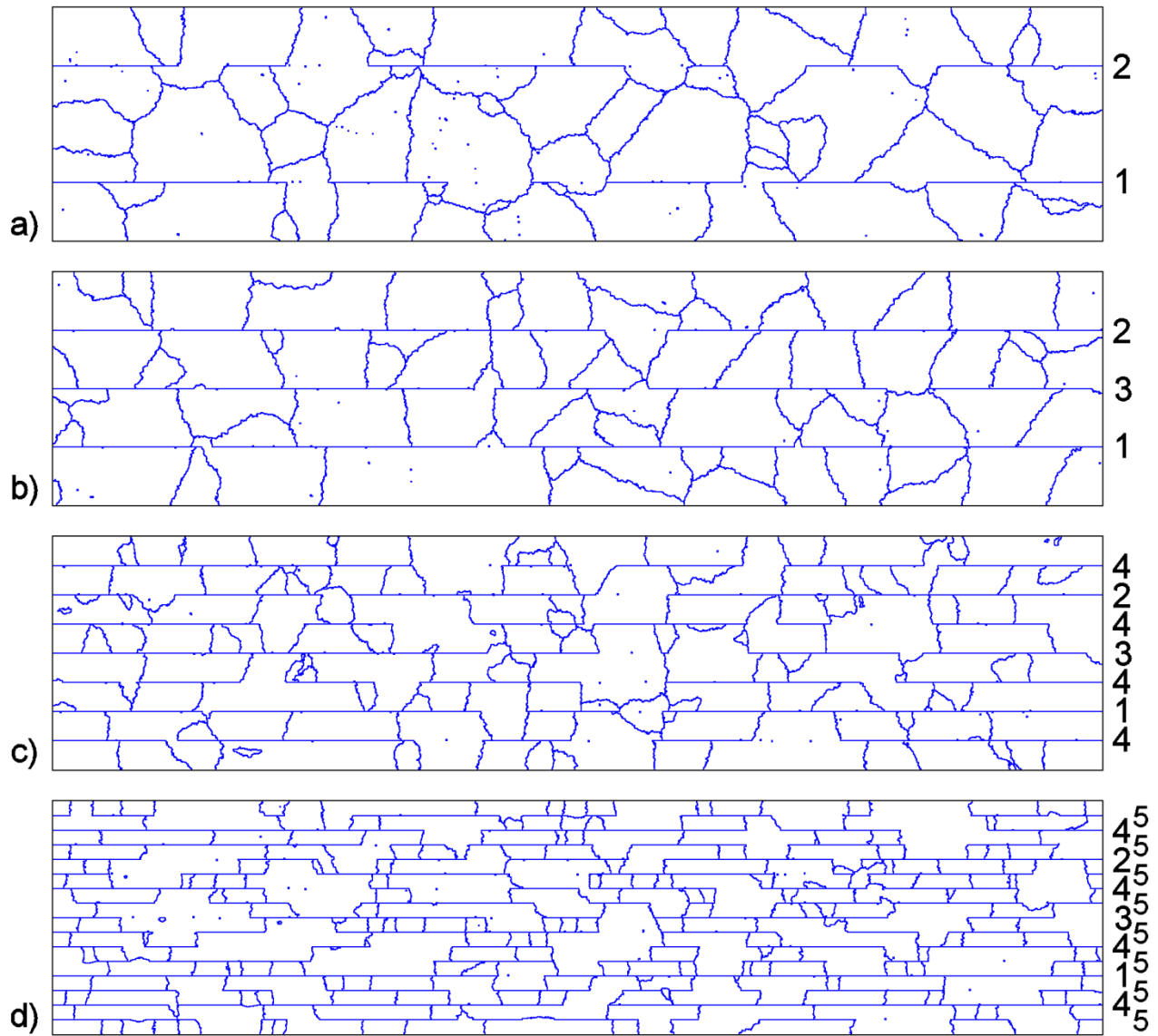
Figure 7. Grain microstructures of the sheets after a) 2, b) 3, c) 4, and d) 5 ARB cycles taken at an annealing time, where the aluminium is fully recrystallized for all cycles.
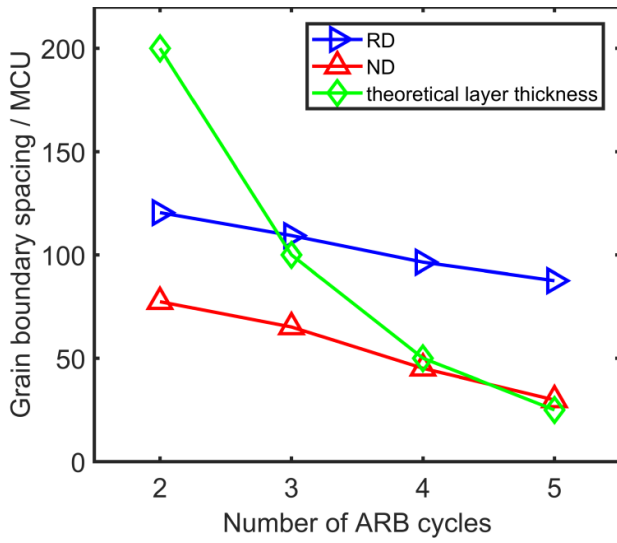
Figure 8. Average grain boundary spacing in RD and ND (from images in Fig. 7) compared with the theoretical layer thickness, analogously to Fig. 3a.
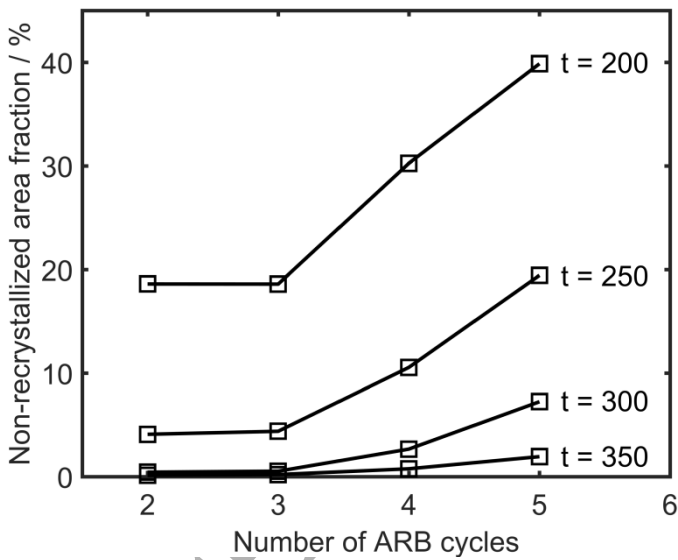

Figure 9. Non-recrystallized volume fraction as a function of applied ARB cycles depending on the annealing time showing for example for $t = 300$ a similar qualitative increase as in Fig. 3b.
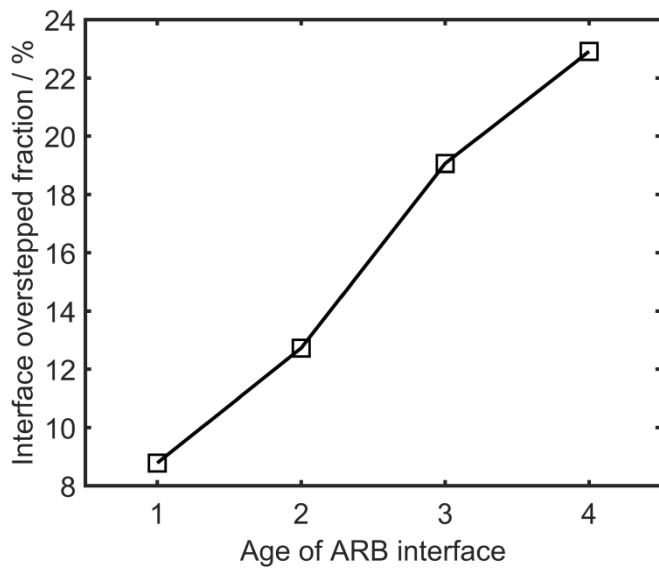
22

Figure 10. Fraction of ARB interfaces crossed by grain boundaries as a function of their age in the sheets of Fig. 7 showing a similar qualitative increase as in Fig. 4.